CHAPTER 3

Synthesis, crystal structure and DNA/protein binding of Tetranuclear Cu(II) complexes with Double-open-cubane like core Framework

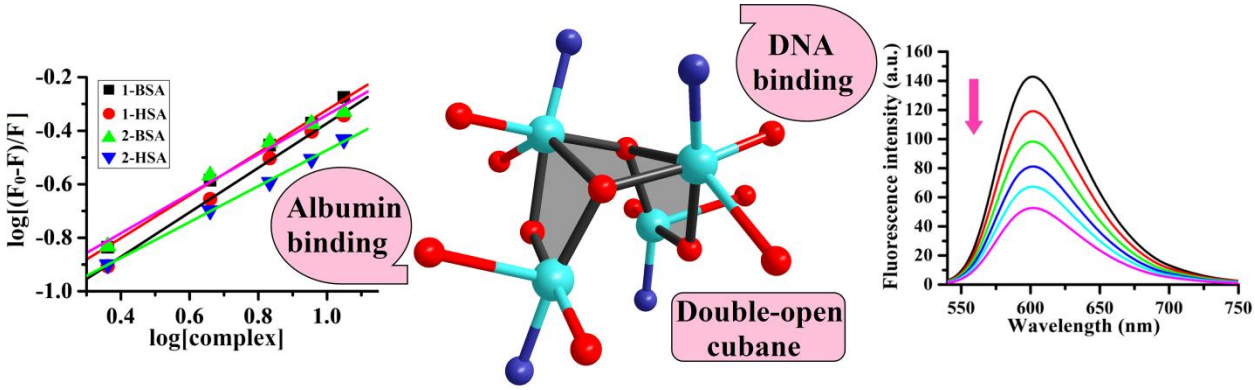

A. Paul et al. / Polyhedron 155 (2018) 447-456

3.1 Introduction

3.2 Experimental

3.2.1 Materials

3.2.2 Physical measurements

3.2.3 X-ray crystallography

3.2.4 Synthesis of ligand and the complexes

3.2.5 Albumin binding studies

3.2.6 DNA binding studies

3.3 Results and discussion

3.3.1 Synthetic aspect

3.3.2 Crystal structures

3.3.3 Electronic absorption and fluorescence spectra of complexes

3.3.4 ESI mass spectroscopy

3.3.5 Protein binding studies

3.3.6 Interaction with Calf-Thymus DNA

3.3.7 Redox properties of the complexes

3.4 Conclusion

3.1 **Introduction**

Transition metal clusters containing paramagnetic metal ions represent important class of compounds for their potential application in the area of molecular magnetism [3.1] and their importance in the field of bioinorganic chemistry, as mimics for multi-metal active sites of metalloproteins [3.2]. Polynuclear copper complexes of various structures e.g. dimeric [3.3a], square planar [3.3b], cyclic [3.3c], pin-wheel [3.3d], roof-shaped [3.3e] and cubane types [3.3f-3.3j] are reported in the literature due to their potential application in the area of magnetism [3.4], catalysis [3.5] and bioinorganic modeling [3.6]. Depending on the arrangement of copper and oxygen atoms in Cu_4O_4 unit various cubane geometries such as regular cubane [3.7], single-open cubane [3.8], double open cubane [3.9] and face-sharing dicubane have been reported [3.9b, 3.10] in the literature. Literature survey reveals that many copper(II) based coordination compounds are used as metallo-pharmaceuticals [3.11] and these compounds play important role in biology due to their antimicrobial [3.12], antifungal [3.13], antibacterial [3.14], antitumoral [3.15], antiviral [3.16], antipyretic [3.13a] and antidiabetic activities [3.17]. DNA is the primary intracellular target of antitumor drugs, since the interaction between small molecules with DNA can cause DNA damage and block DNA synthesis in cancer cells [3.18]. Therefore, under physiological conditions, metal complexes which can capable to binding and cleaving DNA are considered as potential candidates for use as therapeutic agents in medicinal applications [3.19]. On the other hand studies of the binding of metal complexes with serum albumins is important to understand the potential of these compounds as drugs, as the nature and magnitude of binding has direct relation on drug delivery, drug absorption and the therapeutic efficiency [3.20]. Therefore, understanding and characterizing the interaction of drugs with DNA and serum albumin (HSA/BSA) are important for the development of new drugs. It is to note that reported

tetranuclear Cu(II)-cubane complexes mainly focused on the synthesis and magneto-structure correlation [3.4]. Whilst studies of DNA / protein binding on tetranuclear Cu(II)-cubane complexes are rare in the literature [3.3g, 3.3h].

As a part of our continuing work on Cu(II) complexes with Schiff base ligands, in the present contribution we have used a polydentate ligand (H_2L), which function as chelating ligand with its versatile coordination modes (Scheme 3.1), and using H_2L we synthesized two tetranuclear copper(II) complexes, $[Cu_4(L)_2(HL)_2(H_2O)_2]\cdot 2(ClO_4)\cdot 2(H_2O)\cdot DMF$ (**1**) and $[Cu_4(L)_2(HL)_2(H_2O)_2]\cdot(tp)$ (**2**) with double open cubane structure. Interactions of complexes with calf thymus DNA (CT-DNA) and serum albumins (BSA/HSA) have been studied with Uv-vis and fluorescence spectroscopic techniques.

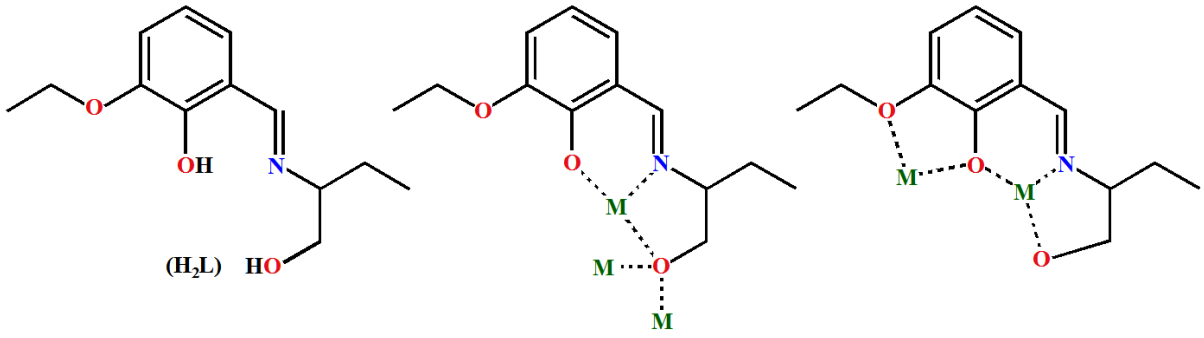

Scheme 3.1 Structure of H_2L, and its coordination modes of in **1**-**2**.

3.2 Experimental

3.2.1 Materials

High purity 2-amino-1-butanol, 2-hydroxy-3-ethoxybenzaldehyde, calf thymus DNA, bovine serum albumin and human serum albumin were purchased from Aldrich Chemical Co. Inc. and used as received. All other chemicals used were analytical grade. Solvents used for spectroscopic studies were purifies and dried by standard procedures before use [3.21].

3.2.2 Physical measurements

Elemental analyses, IR spectra, NMR spectra of ligand and electronic absorption spectra were recorded according to the previous chapter. ESI-MS spectra of the compounds were recorded on an Agilent Q-TOF 6500 mass spectrometer and the software used for mass analysis is Mass hunter. Emission spectra were recorded on a Hitachi F-7000 spectrofluorimeter. Room temperature (300 K) spectra were obtained in methanolic solution using a quartz cell of 1 cm path length. The slit width was 5 nm for both excitation and emission.

The fluorescence quantum yield was determined using phenol as a reference and methanol medium for both complexes and reference. Emission spectra were recorded by exciting the complex and the reference phenol at the same wavelength, maintaining nearly equal absorbance (~ 0.1). The area of the emission spectrum was integrated using the software available in the instrument and the quantum yield calculated [22] according to the following equation:

$$\Phi_s = \Phi_r \frac{A_s}{A_r} \frac{I_r}{I_s} \frac{\eta_s^2}{\eta_r^2}$$

Where Φ_s and Φ_r are the fluorescence quantum yield of the sample and reference, respectively. A_s and A_r are the respective optical densities at the wavelength of excitation, I_s and I_r correspond to the areas under the fluorescence curve; and η_s and η_r are the refractive index values for the sample and reference, respectively. The fluorescence enhancement efficiency (%) was calculated by using equation $[(F - F_o)/F_o] \cdot 100$ and the corresponding quenching efficiency (%) by $[(F_o - F)/F_o] \cdot 100$, where F_0 and F are the maximum fluorescence intensity of the complex before exposure and in presence of the analyte, respectively. Stern-Volmer equation $F_0/F = 1 + K_{sv}[complex]$ (where F_0 and F are the fluorescence intensities in absence and in presence of the

complexes, K_{sv} is Stern-Volmer constant) was used to explain the fluorescence quenching phenomenon [3.22].

Electrochemical measurements performed under a dry argon atmosphere with a BAS Epsilon electrochemical system. A three-electrode assembly comprising a glassy carbon (for reduction) or Pt (for oxidation) working electrode, Pt auxiliary electrode, and an aqueous Ag/AgCl reference electrode were used. Cyclic voltammetric (CV) measurements were carried out at 298 K using methanolic solution of complexes (ca. 1 mM) and the concentration of supporting electrolyte tetraethylammonium perchlorate (TEAM) was maintained at 0.1 M. The potentials reported were referenced against the Ag/AgCl electrode, which under given experimental conditions gave a value of 0.36 V for ferrocene/ferrocenium couple.

3.2.3 X-ray crystallography

Data collections of complexes **1** and **2** were carried out at 120 K on an Oxford Diffraction Gemini Ultra diffractometer. Cell refinement, indexing and scaling of the data sets were done with CrysAlisPro package, Version 1.171.35.10 [3.23]. The structures were solved by using the olex2.solve solution program [3.24] using the charge flipping algorithm and refined by the full matrix least-squares method based on F^2 with all observed reflections [3.25]. All the calculations were performed using the WinGX [3.26]. For **1** three of the four ligands exhibit some form of disorder in the side-chains. This disorder has been modeled in two sets (PART 1 and PART 2) with occupancy of 0.6 and 0.4. One of the perchlorates is also disordered in the same ratios. Standard methods to restrain distances and also some ADPs have been employed. These restraints are detailed in the embedded res file and also described explicitly in a textual way. The restraints did not affect the R factors in a negative way. Packing diagrams were done with graphical program Diamond [3.27]. Crystal data and details of refinements are given in Table

3.1. The cif file CCDC numbers are 1544798 and 1544799 for complex **1** and complex **2**, respectively.

Table 3.1 Crystal data and structure refinement of complexes **1**-**2**.

Complex	**1**	**2**
Empirical formula	$C_{55}H_{85}Cu_4N_5O_{25}Cl_2$	$C_{60}H_{78}Cu_4N_4O_{18}$
Formula mass, g mol^{-1}	1541.33	1397.46
Crystal system	Triclinic	Triclinic
Space group	*P-1*	*P-1*
a, Å	11.6628(6)	13.1269(12)
b, Å	14.0257(7)	15.7400(15)
c, Å	20.9237(6)	16.5893(11)
α, deg	93.892(3)	93.042(7)
β, deg	98.319(3)	104.161(7)
γ, deg	107.142(4)	110.732(9)
V, $Å^3$	3214.0(3)	3071.2(5)
Z	2	2
$D_{(calcd)}$, g cm^{-3}	1.577	1.509
μ(Mo-Kα), mm^{-1}	1.472	1.441
F(000)	1582	1448
Theta range, deg	1.9, 25.0	1.8, 25.0
No. of collected data	47359	29770
No. of unique data	11315	10798
R_{int}	0.085	0.093
Observed reflns [$I > 2\sigma(I)$]	8532	5375
Goodness of fit (F^2)	1.073	1.020
Parameters refined	11315, 1041	10798, 783
*R*1, *wR*2 ($I > 2\sigma(I)$) [a]	0.0727, 0.1732	0.0918, 0.2707
Residuals, e $Å^{-3}$	-1.38, 1.53	-0.59, 0.88

[a] $R1(Fo) = \Sigma \left| \left| Fo \right| - \left| Fc \right| \right| / \Sigma \left| Fo \right|$, $wR2(Fo^2) = [\Sigma w (Fo^2 - Fc^2)^2 / \Sigma w (Fo^2)^2]^{½}$

3.2.4 Synthesis of ligand and complexes

Synthesis of 2-ethoxy-6-[(1-hydroxymethyl-propylimino)-methyl]-phenol (H_2L)

A methanolic solution (50 ml) of 1:1 mixture of 2-aminobutanol (1 mmol, 0.089 g) and 2-hydroxy-3-ethoxybenzaldehyde (1 mmol, 0.166 g) was refluxed for 3 h. The resulting yellow color solution cooled to room temperature and solid yellow compound was obtained after evaporation of solvent. Re-crystallization of compound using methanol as solvent results yellow crystals. Crystalline solid was collected by filtration and dried in air to afford H_2L. Yield: Yield 0.197 g (83%). Anal. calc. for $C_{13}H_{19}NO_3$ (237.29): C, 65.80; H, 8.07; N, 5.90 %. Found: C, 65.82; H, 8.11; N, 5.22 (%).^{1}H NMR (400 MHz, $CDCl_3$, δ ppm): 0.796-0.877 (6H, m), 1.414 - 1.432 (2H, m), 2.586 (1H, s), 3.147 - 3.190 (1H, m), 3.559 - 3.683 (2H, m), 4.013 - 4.048 (2H, m), 4.863 (1H, s), 6.671 - 6.850 (1H, d; 2H, m), 8.271 (1H, s). ^{13}C NMR ($CDCl_3$, 100 MHz, δ ppm): 153.71 (Ar-C-OH), 165.37 (-CH=N-), 147.96 (C-OEt), 123.08, 118.08, 117.40, 115.29 (Ar-C), 72.14 (-CH_2-OH), 66.28 (=N-CH-), 64.34 (-O-CH_2), 24.98 (-CH_2-), 14.83 (-CH_3 of -OEt), 10.35 (-CH_3).

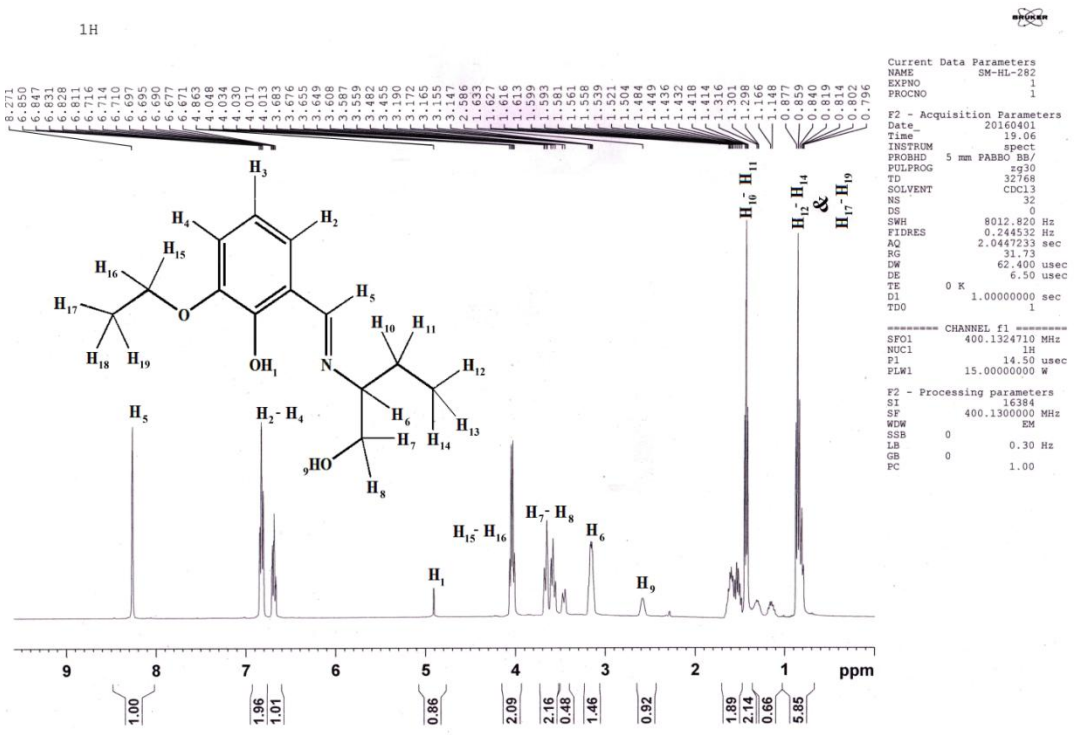

Fig. 3.1 ^{1}H NMR spectra of H_2L.

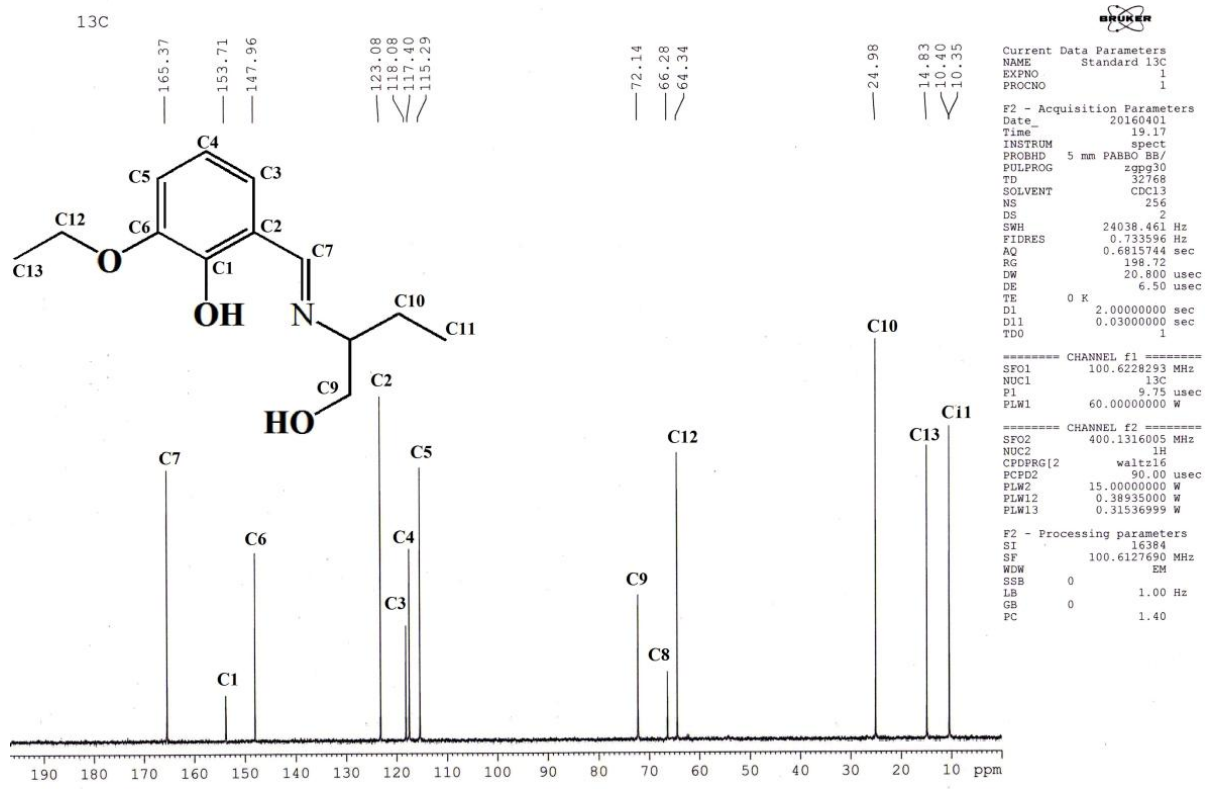

Fig. 3.2 ^{13}C NMR spectra of H_2L.

Synthesis of complexes:

Caution! *Perchlorate salts of metal with organic ligands are potentially explosive. Only a small amount of material should be prepared, and it should be handled with care.*

The complexes have been synthesized by adopting the procedures schematically given in Scheme 3.2.

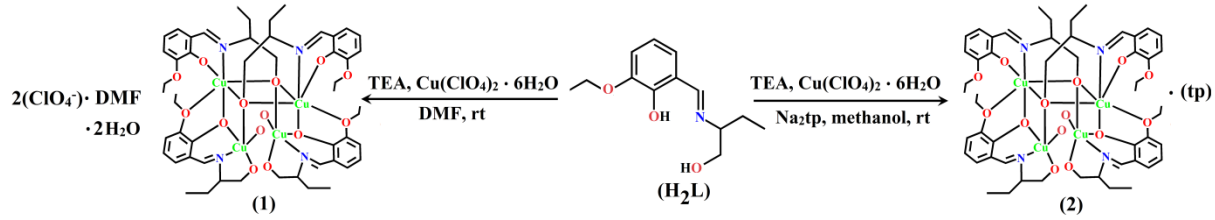

Scheme 3.2 Synthesis of **1** and **2**.

[Cu$_4$(L)$_2$(HL)$_2$(H$_2$O)$_2$]·2(ClO$_4$)·2(H$_2$O)·DMF (1)

A methanolic solution (15 ml) of (1:1) mixture of triethylamine (1 mmol, 0.101 g) and H_2L (1 mmol, 0.237 g) was added drop wise to a methanolic-DMF (1:1) solution (10 ml) of copper perchlorate hexahydrate (1 mmol; 0.370 g) under stirring condition. The whole deep green reaction mixture was stirred for additional 2 hours and filtered. The filtrate was kept in open atmosphere for slow evaporation and green single crystals suitable for X-ray diffraction quality were obtained after a few days. Yield: 81%. Anal. calc. for $C_{55}H_{85}Cu_4N_5O_{25}Cl_2$ (1541.33): C,42.86; H, 5.56; N, 4.54 %. Found: C, 42.84; H, 5.38; N, 4.53 (%). IR (cm^{-1}): 3430 (vs), 2984 (vw), 1642 (vs), 1550 (vs), 1466 (s), 1413 (vs), 1373 (w), 1244 (vw), 1300 (s), 1078 (s), 882 (vw), 632(vw).

[Cu$_4$(L)$_2$(HL)$_2$(H$_2$O)$_2$]·(tp) (2)

A methanolic solution (15 ml) of (1:1) mixture of triethylamine (1 mmol, 0.101 g) and H_2L (1 mmol, 0.237 g) was added drop wise to a methanolic (1:1) solution (10 ml) of copper perchlorate hexahydrate (1 mmol; 0.370 g) under stirring condition. To the resulting green solution an aqueous solution of sodium terephthalate (1 mmol, 0.21g) was added after 2 hours and stirred additional 1 hour and filtered. The filtrate was kept in air for slow evaporation at room temperature and green single crystals suitable for X-ray diffraction quality were obtained after a few days. Yield: 76%. Anal. calc. for $C_{60}H_{78}Cu_4N_4O_{18}$ (1397.46): C, 51.57; H, 5.63; N, 4.01 %. Found: C, 51.82; H, 5.34; N, 4.07 (%). IR (cm^{-1}): 3435 (vs), 2984 (vw), 1644 (vs), 1551 (vs), 1466 (s), 1414 (vs), 1373 (s), 1300 (s), 1244 (vw), 1079 (s), 882 (vw), 664 (vw).

3.2.5 Albumin binding studies

Stock solutions of human serum albumin (HSA) and bovine serum albumin (BSA) were prepared in HEPES buffer (pH 7.2). The stock solutions of complexes were prepared by

dissolving the complexes in water. The absorption titration experiments were carried out by keeping the concentration of SA constant (4.75×10^{-5} M for BSA; 3.16×10^{-5} M for HSA), while varying the concentrations of Cu(II) complexes (0 to 11.2 μM). The interactions of compounds with serum albumins were studied by recording the tryptophan fluorescence of HSA / BSA. To the solutions of serum albumin, the Cu(II) complexes were added at room temperature, and the quenching of emission intensities at 340 nm (λ_{ex}, 280 nm) for BSA and 330 (λ_{ex}, 280 nm) for HSA were recorded after gradual addition of (20μL, 0.3475mmol) aqueous solution of complexes. Stern-Volmer constant (K_{sv}) and quenching rate constant (k_q) were calculated using Stern-Volmer equation and the relation $K_{sv} = k_q\tau_0$, where τ_0 is the fluorescence lifetime [3.28] of the tryptophan residue of serum albumin (~ 5×10^{-9} s). The binding constant (K_{bin}) and the number of binding sites (n) were calculated using the following Scatchard equation [3.29]. Where [complex] is the total concentration of the added complex.

$$\log[(F_o–F)/F] = \log K_{bin} + n \log[complex]$$

3.2.6 DNA binding studies

Electronic absorption spectral study

The binding of complexes with CT-DNA were studied by UV-vis spectroscopy to determine possible DNA-binding modes and binding constant. The UV spectra of the complexes were recorded with a fixed concentration of the complexes (5 μM) in water and varying the concentration of CT-DNA (0 - 15.48 μM) at room temperature in HEPES buffer (P^H = 7.2). Intrinsic binding constants (K_{ib}) of the complexes with CT-DNA were determined using the equation [3.30]

$$\frac{[DNA]}{(\varepsilon_a - \varepsilon_f)} = \frac{[DNA]}{(\varepsilon_b - \varepsilon_f)} + \frac{1}{K_{ib}(\varepsilon_b - \varepsilon_f)}$$

where [DNA] is the concentration of CT-DNA, and ε_a is the extinction co-efficient value of the complex at a given CT-DNA concentration. ε_f and ε_b are the extinction co-efficient of the complex only and when fully bound to CT-DNA, respectively. A plot of [DNA]/($\varepsilon_a - \varepsilon_f$) vs [DNA] gives a straight line with $\frac{1}{(\varepsilon_b - \varepsilon_f)}$ and $\frac{1}{K_{ib}\,(\varepsilon_b - \varepsilon_f)}$ as slope and intercept, respectively. From the ratio of the slope to the intercept the value of K_{ib} were calculated.

Competitive binding fluorescence measurement

Ethidium bromide competitive studies of each compound were carried out with the fluorescence spectroscopy to examine whether the tested compounds **1** and **2** can displace EB from the CT-DNA bound EB system. Aqueous solution of EB bounded CT-DNA (8 μM) solution prepared in HEPES buffer (pH 7.2). In the presence of DNA, ethidium bromide (EB) exhibits fluorescence (λ_{em} = 602 nm, λ_{ex} = 500 nm) enhancement due to its intercalative binding to DNA. Competitive binding of the copper compound with CT-DNA results fluorescence quenching due to displacement of EB from CT-DNA. The DNA-intercalating effect of **1** and **2** were studied by gradual addition of complexes (20 μL, 0.3475 mmol) to the EB-DNA complex. The fluorescence intensities of EB bounded CT-DNA were recorded with increasing concentration of Cu(II) complexes.

3.3 **Results and discussion**

3.3.1 Synthetic aspect

The multisite coordinating ligand, H_2L, was prepared by a one pot synthesis employing the condensation of 2-amino-1-butanol and 2-hydroxy-3-ethoxybenzaldehyde in methanol under refluxing condition, and characterized by ^{1}H and ^{13}C NMR spectra (Figs. 3.1 and 3.2). Using H_2L, complexes **1** and **2** were synthesized at room temperature.

3.3.2 Crystal structures

The molecular structures of **1** and **2** are shown in Figs. 3.3 and 3.4. Selected bond lengths and angles are listed in Table 3.2. Both the complexes crystallize in the triclinic system with the P-1 space group.

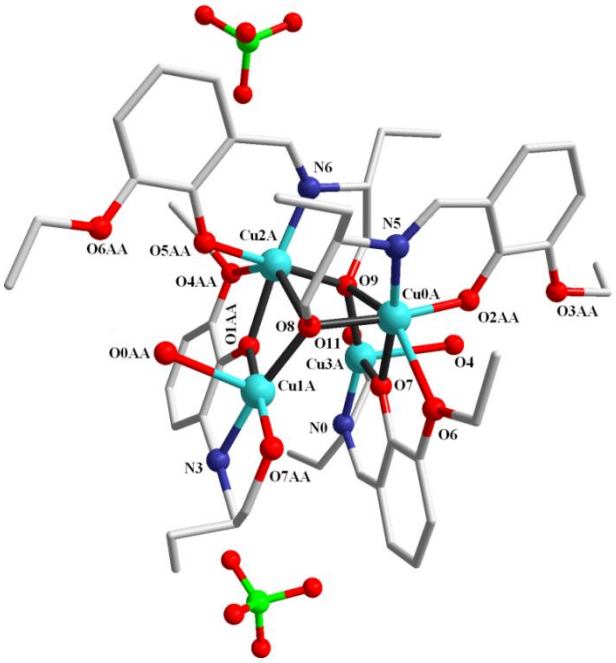

Fig. 3.3 Molecular structure of **1** (lattice DMF, H_2O molecules and hydrogen atoms are omitted). Only one out of the two orientations of the disordered perchlorate anion and one out of two disordered $–CH_2$-CH_3 side chains of three Schiff base are shown for clarity.

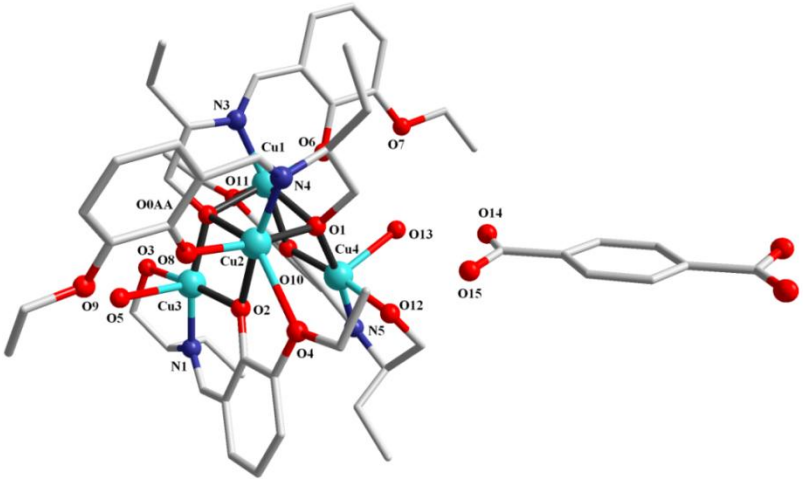

Fig. 3.4 Molecular structure of **2.** The hydrogen atoms are omitted for clarity.

Table 3.2 Coordination bond lengths (Å) and angles (º) for complexes **1-2**.

1		**2**	
Bond lengths			
Cu(0A)-O(2AA)	1.912(5)	Cu(1)-O(1)	2.449(7)
Cu(0A)-O(6)	2.433(4)	Cu(1)-O(0AA)	1.953(7)
Cu(0A)-O(7)	1.991(4)	Cu(1)-O(6)	1.902(7)
Cu(0A)-O(8)	1.963(5)	Cu(1)-O(10)	2.005(8)
Cu(0A)-O(9)	2.582(4)	Cu(1)-O(11)	2.563(8)
Cu(0A)-N(5)	1.940(5)	Cu(1)-N(3)	1.943(12)
Cu(1A)-O(1AA)	1.944(5)	Cu(2)-O(1)	1.941(7)
Cu(1A)-O(8)	1.918(4)	Cu(2)-O(0AA)	2.500(8)
Cu(1A)-O(0AA)	2.327(5)	Cu(2)-O(2)	2.021(7)
Cu(1A)-O(7AA)	2.017(5)	Cu(2)-O(4)	2.528(8)
Cu(1A)-N(4)	1.913(19)	Cu(2)-O(8)	1.912(7)
Cu(2A)-O(1AA)	2.016(4)	Cu(2)-N(4)	1.940(9)
Cu(2A)-O(5AA)	1.911(5)	Cu(3)-O(0AA)	1.919(7)
Cu(2A)-O(4AA)	2.429(5)	Cu(3)-O(2)	1.979(7)
Cu(2A)-O(8)	2.520(4)	Cu(3)-O(3)	2.018(8)
Cu(2A)-O(9)	1.955(5)	Cu(3)-O(5)	2.263(7)
Cu(2A)-N(6)	1.940(5)	Cu(3)-N(1)	1.934(10)
Cu(3A)-O(4)	2.372(6)	Cu(4)-O(1)	1.921(7)
Cu(3A)-O(7)	1.942(5)	Cu(4)-O(10)	1.962(8)
Cu(3A)-O(9)	1.917(4)	Cu(4)-O(12)	1.973(10)
Cu(3A)-O(11)	2.009(6)	Cu(4)-O(13)	2.271(7)
Cu(3A)-N(2)	1.983(18)	Cu(4)-N(5)	1.906(13)
Bond angles			
Cu(0A)-O(7)-Cu(3A)	109.3(2)	Cu(1)-O(1)-Cu(2)	97.1(3)
Cu(0A)-O(8)-Cu(2A)	92.06(18)	Cu(1)-O(1)-Cu(4)	91.3(2)
Cu(1A)-O(8)-Cu(2A)	91.21(16)	Cu(2)-O(1)-Cu(4)	120.1(3)
Cu(0A)-O(8)-Cu(1A)	124.5(2)	Cu(1)-O(0AA)-Cu(2)	95.2(3)
Cu(2A)-O(9)-Cu(3A)	123.2(2)	Cu(1)-O(0AA)-Cu(3)	119.9(4)
Cu(0A)-O(9)-Cu(2A)	90.41(18)	Cu(2)-O(0AA)-Cu(3)	91.6(3)
Cu(0A)-O(9)-Cu(3A)	89.66(16)	Cu(2)-O(2)-Cu(3)	106.0(4)

The core structures of both complexes are the same and the only difference is the presence of different lattice molecules (two perchlorate ions and one DMF molecule in **1**, compared to one terephthalate ion in **2**). Both the complexes possess a double open cubane core structure. The tetranuclear cubane core consist of four copper(II) centers, two dideprotonated Schiff base ligands [L^{2-}] and two monodeprotonated Schiff base ligands [HL^{-}]. Each HL^{-} ligand chelates two

copper atoms *via* μ_2-η^1:η^1:η^1:η^2-*O,O,N,O* coordination mode, while the L^{2-} ligand chelates the other two copper centers along with connecting to the previous moieties with a μ_3-alkoxido group resulting in the μ_3-η^1:η^1:η^3-*O,N,O* coordination mode, while the ethoxy oxygen atoms remain uncoordinated. Fig. 3.5 and Fig. 3.6 show simplified representation of the coordination environment around the four copper centers of **1** and **2**, respectively.

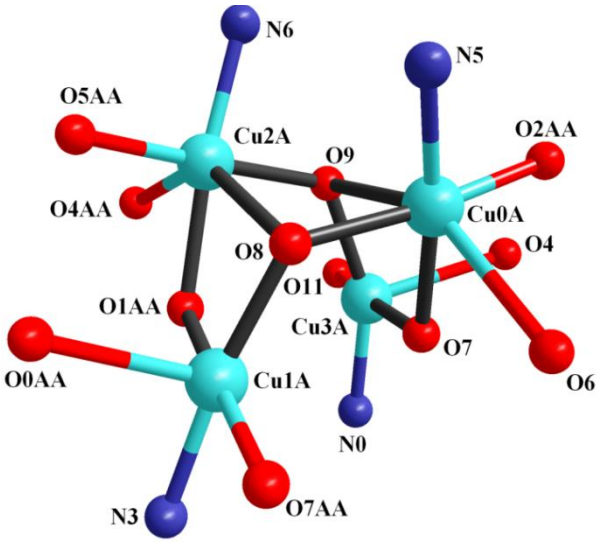

Fig. 3.5 Simplified representation of the tetranuclear copper(II) core in **1**.

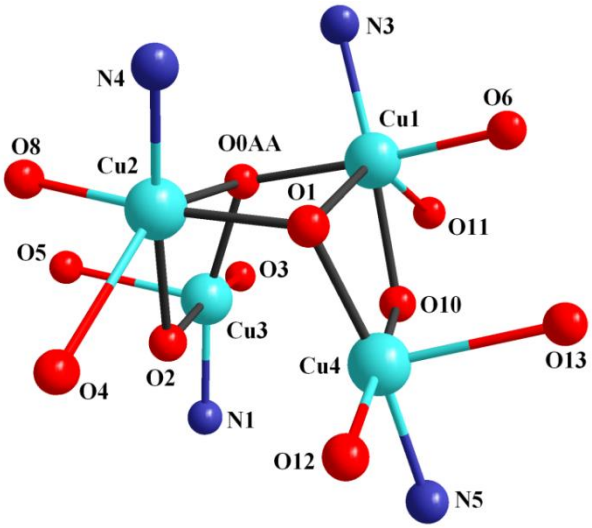

Fig. 3.6 Simplified representation of the tetranuclearcopper(II) core in **2**.

For both the complexes, two copper ions are present in a distorted square pyramidal [Cu(1A) and Cu(3A) for **1**; Cu(3) and Cu(4) for **2**] geometry, whereas the other two metal centers are present in a distorted octahedral geometry [Cu(0A) and Cu(2A) for **1**; Cu(1) and Cu(2) for **2**]. The trigonality parameters [3.31] for five coordinated copper centers are calculated as (α-β)/60, where α and β are the two largest coordination bond angles. Hence a regular TBP structure with D_{3h} symmetry has $\tau_5 = 1$ and for a regular C_{4v} SP geometry $\tau_5 = 0$. The calculated τ_5 values were 0.252 (Cu(1A)), 0.06 (Cu(3A)) for **1,** and 0.156 (Cu(3)), 0.026 (Cu(4)) for **2**. This result indicates that the copper centers possess distorted square pyramidal geometries. The basal planes of the square pyramid for both the complexes are formed by the imine nitrogen, phenoxide oxygen and alcoholic oxygen atoms of the mono deprotonated HL^- ligand and the μ_3-alkoxido oxygen atom of the L^{2-} ligand. The coordinated water molecule occupied the apical position of the square pyramid. The basal coordination bond lengths of the square pyramid are in between 1.913(19) - 2.017(5) Å for **1** and 1.906(13)-2.018(8) Å for **2**. The apical bond lengths are somewhat more distant, being at 2.327(5) Å for Cu(1A) and 2.372(6) Å for Cu(3A), respectively in **1**, whereas they are 2.263(7) Å (for Cu(3)) and 2.271(7) Å(for Cu(4)) in **2** (Table 2). The coordination environment of other two metal centers [Cu(0A), Cu(2A) for **1** and Cu(1), Cu(2) for **2**] remain distorted octahedral. The basal planes of the octahedron are formed by the imine nitrogen, phenoxido and alkoxido oxygen atoms from one $(L)^{2-}$ ligand and μ_2-phenoxido oxygen atoms of the $(HL)^-$ ligand and the axial positions are the occupied by ethoxy oxygen atom of the same $(HL)^-$ ligand and the alkoxido oxygen atom of another $(L)^{2-}$ ligand. The equatorial bond distances are in the range 1.911(5) - 2.016(4) Å for **1** and 1.902(7) - 2.021(7) Å for **2**, while relatively larger (due to Jahn-Teller distortion) the axial bond lengths vary from 2.429(5) to 2.582(4) Å for **1** and 2.449(7) to 2.563(8) Å for **2**. The long Cu(1A)-O(7) (3.039 Å) and Cu(3A)-

O(1AA) (2.991 Å) distances in **1** and Cu(3)-O(10) (3.003 Å) and Cu(4)-O(2) (2.959 Å) for **2** are responsible for the formation of the double open cubane core structure. The copper atoms are located at the vertices of a distorted tetrahedron with edge dimension ranges of 3.199(12) to 3.888(12) Å for **1** and 3.147(23) to 3.891(20) Å for **2** (Figs. 3.7 and 3.8).

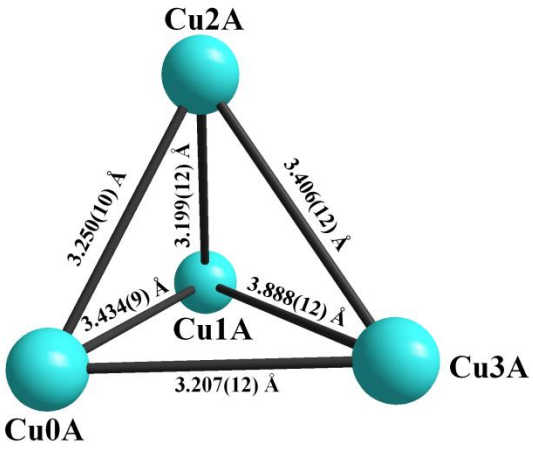

Fig. 3.7 Arrangement of four copper atoms in complex **1**.

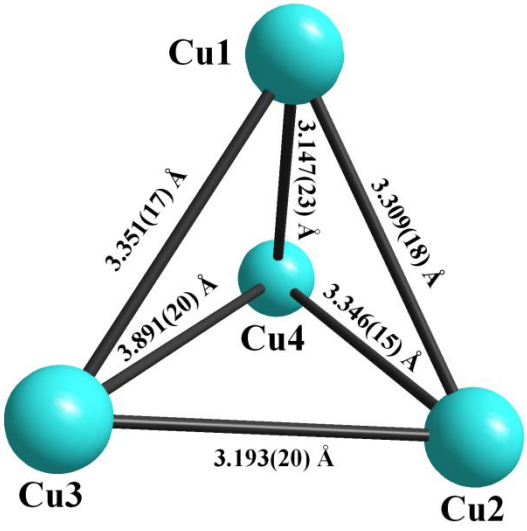

Fig. 3.8 Arrangement of four copper atoms in complex **2**.

Based on the Cu…Cu distances within the Cu_4O_4 cubane core, Alvarez et al. classify [3.32] copper cubane into three types: (i) (2+4), where the Cu…Cu distances are two short and four long; (ii) (4+2), where the Cu…Cu distances are two long and four short; and (iii) (6+0), where

the six Cu…Cu distances of the Cu_4O_4 cubane core are similar [3.32c]. However in complex **1**, the Cu…Cu distances are 3.199(12), 3.250(10), 3.207(12), 3.406(12), 3.434(9) and 3.888(12) Å, and in **2**, Cu…Cu distances are 3.147(23), 3.193(20), 3.891(20), 3.346(15), 3.351(17) and 3.309(18) Å. The Cu…Cu distances in **1** and **2** indicate that the Cu_4O_4 cubane cores of these complexes do not belong to any of the above categories as proposed by Alvarez et al.

In the packing of **1** the tetrameric units are connected through C-H...π interaction [3.33] (C-H...Cg = 2.898 Å) and form 1D supramolecular chain. These 1D chains are again interconnected through two different types hydrogen bonding interaction (C2EA-HA...O4 = 2.101 and C2EA-HB...O0AA = 2.211 Å) and finally form 2D supramolecular architecture (Fig. 3.9).

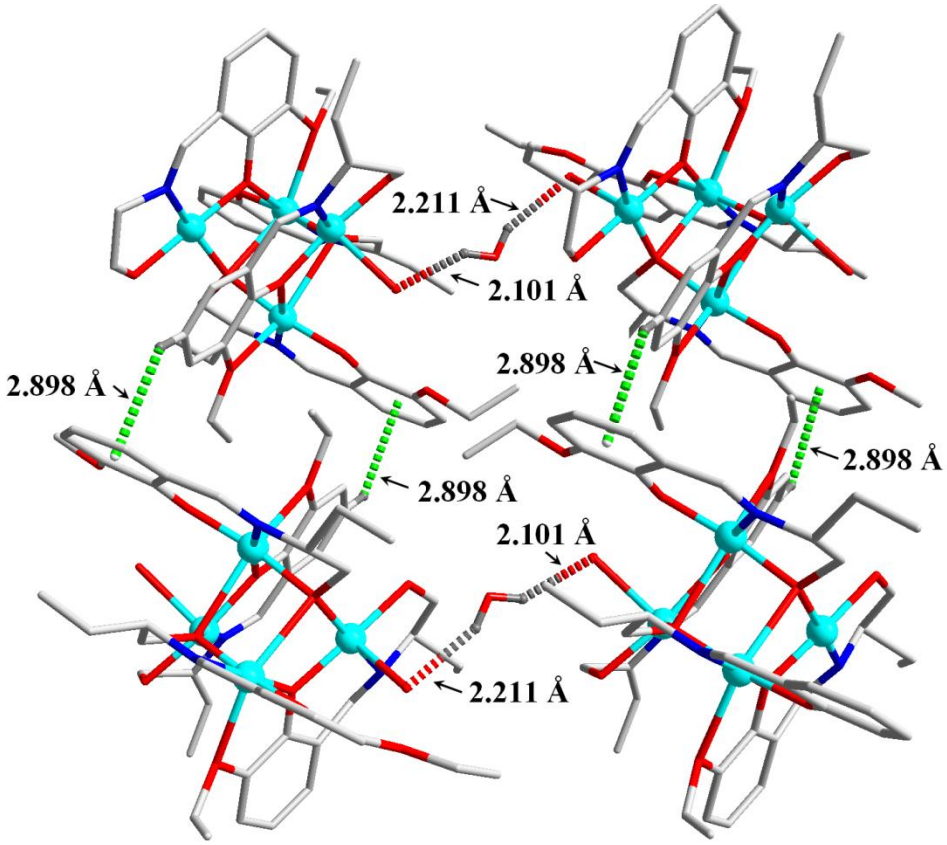

Fig. 3.9 2D supramolecular structure of **1** formed by hydrogen bonding and C-H…π interactions.

On the other hand packing diagram of **2** indicates that it exist as a 3D layer through three different types of C-H...π interactions (Fig. 10; C-H...Cg = 2.747 Å, 3.262 Å and 3.302 Å).

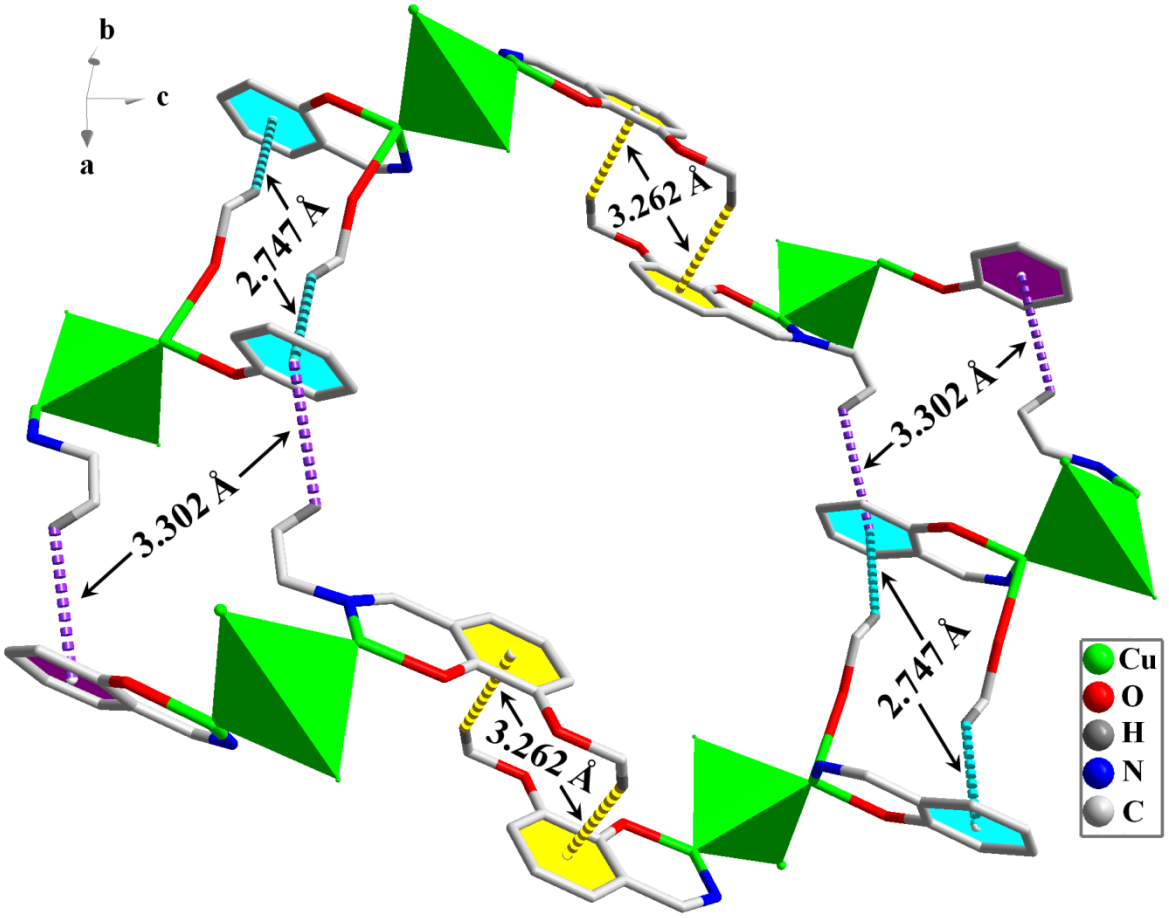

Fig. 3.10 Simplified representation of C-H…π interactions in complex **2**.

Here tetrameric units are interconnected through C-H...π (C-H...Cg = 2.747 Å) interaction to form 1D supramolecular chain, and these 1D chains are again connected through another type C-H...π interaction (C-H...Cg = 3.262 Å) which result 2D supramolecular layer structure. These 2D supramolecular layers are further connected through a different type C-H...π interaction (C-H...Cg = 3.302 Å) and finally form 3D supramolecular structure. The lattice terephthalate ions in complex **2** form 1D supramolecular chains through four different types hydrogen bonding interactions [O(3)-H(3)...O(17) = 1.73, O(5)-H(5B)...O(16) = 1.98, O(12)-H(12)...O(15) = 1.84 and O(13)-H(13A)...O(14) = 1.78 Å] with cubane units (Fig. 3.11).

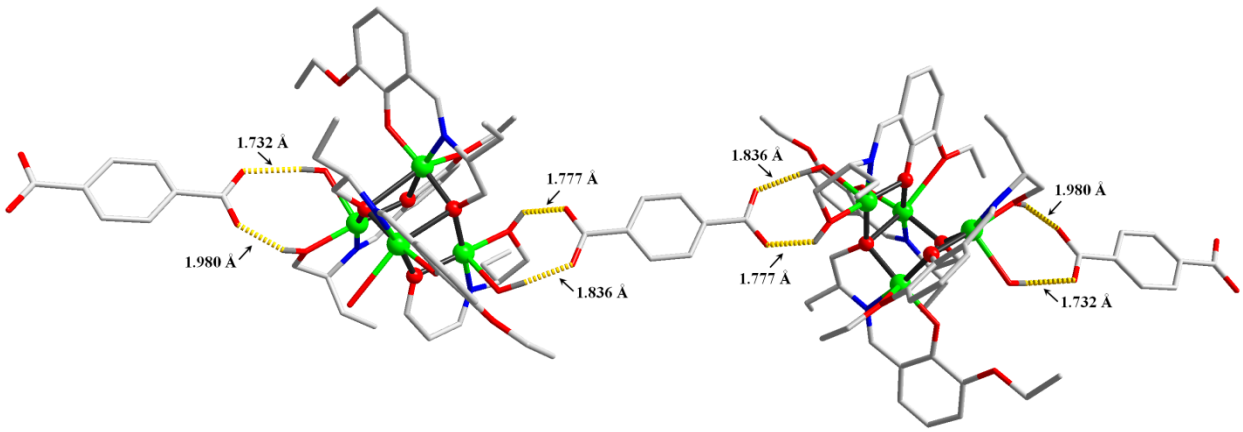

Fig. 3.11 1D supramolecular structure of **2,** formed by hydrogen bonding interactions with lattice terephthalate anion.

3.3.3 IR spectra of complexes

IR spectra of complexes **1** and **2** are shown in Figure 3.12 and 3.13. Both the complexes exhibit a strong broad bands in the region 3200 - 3600 cm^{-1} due to the ν(O-H) stretching vibration [3.34]. The bands at 2984 cm^{-1} for both complexes corresponds to the aromatic ν(C-H) stretching vibrations and aliphatic ν (C-H) stretching vibrations for **1** and **2** appears at 2944 cm^{-1} and 2945 cm^{-1} respectively. Asymmetric and symmetric stretching vibrations of the carboxylate group for **2** appear at 1644 cm^{-1} and 1414 cm^{-1}, respectively. Separation between asymmetric and symmetric stretching (Δν) vibration for **2** is 230 cm^{-1}, which is very close to the Δν of sodium salt of terephthelic acid (Δν = 227 cm^{-1}) [35], indicating the presence of free carboxylate in **2**. The strong and sharp bands at 1550 cm^{-1} for **1** and 1551 cm^{-1} for **2** are due to the aliphatic (C=N) stretching vibration. For both **1** and **2** the band at 1244 cm^{-1} corresponding to ν(O-Et) stretching vibrations. The bands at 882 cm^{-1} (ρ_r) and 632 cm^{-1} (ρ_w) (for **1**) and appears at 882 cm^{-1} (ρ_r) and 664 cm^{-1} (ρ_w) (for **2**) indicate the presence of coordinated water molecules in **1** and **2**.

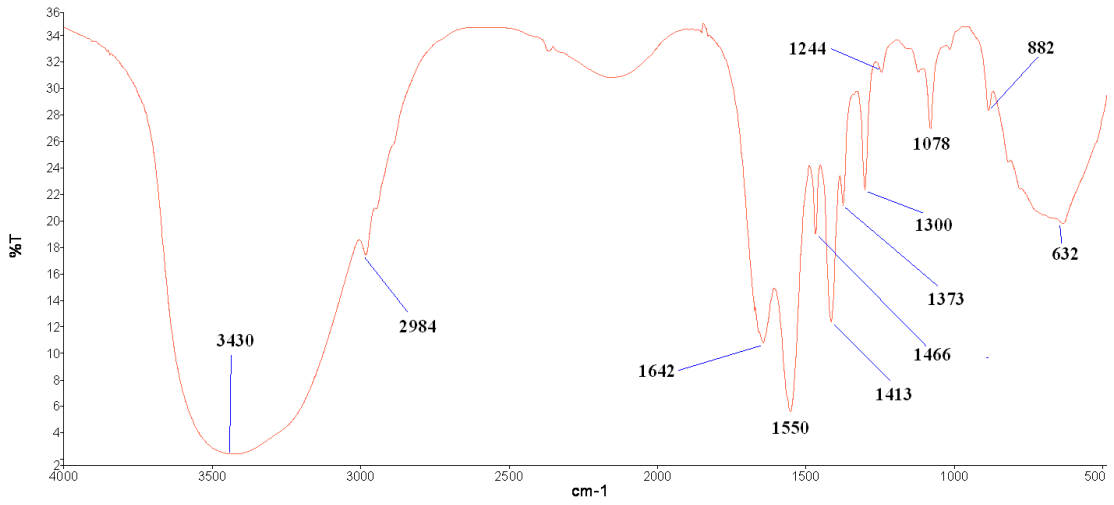

Fig. 3.12 IR spectrum of complex **1**.

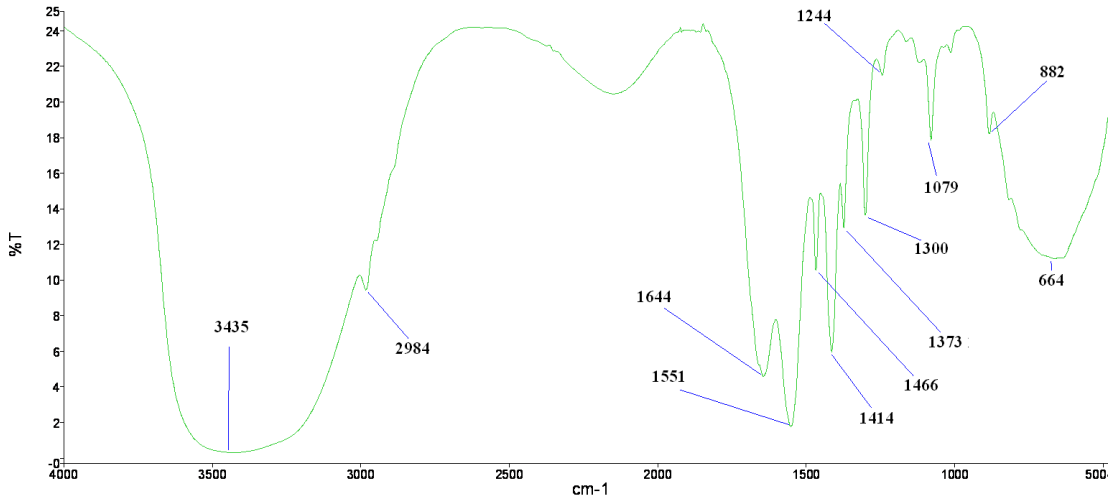

Fig. 3.13 IR spectrum of complex **2**.

3.3.4 Electronic absorption and fluorescence spectra of complexes

The electronic absorption spectra of the complexes show (Fig. 3.14) significant transitions at 231 nm ($\varepsilon \sim 8.82 \times 10^4$ liter mole^{-1} cm^{-1} for **1** and 6.14×10^4 liter mole^{-1} cm^{-1} for **2**), 276 nm ($\varepsilon \sim 4.62 \times 10^4$ liter mole^{-1} cm^{-1} for **1** and 2.94×10^4 liter mole^{-1} cm^{-1} for **2**) and 370 nm ($\varepsilon \sim 1.3 \times 10^4$ liter mole^{-1} cm^{-1} for **1** and 8.0×10^3 liter mole^{-1} cm^{-1} for **2**). The results of the study on the luminescence properties are summarized in Table 3.3.

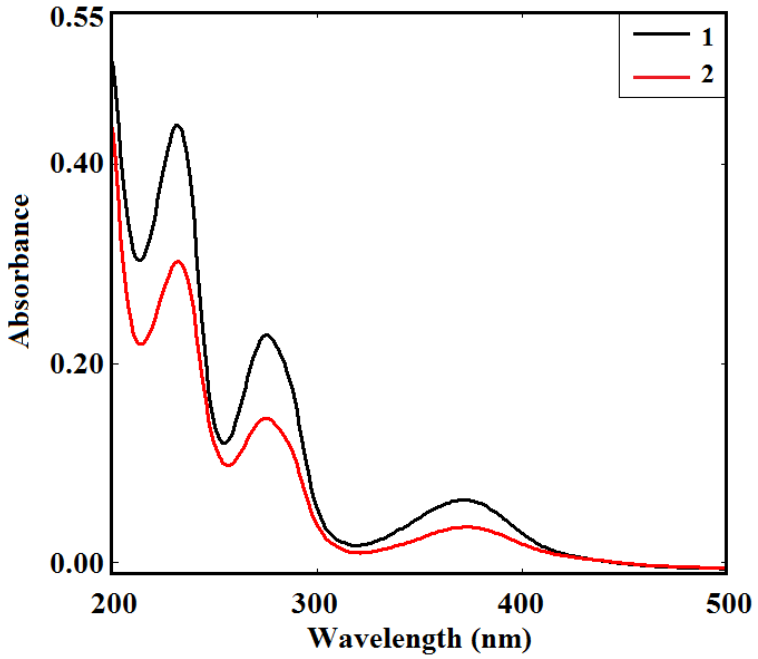

Fig. 3.14 Electronic absorption spectra of complexes**1** and **2**.

Both the complexes exhibit red shifted emission. On excitation at 370 nm, complex **1** exhibits a sharp emission band at 430 nm and two weak shoulders at 458 and 572 nm. Whereas, for complex **2** upon excitation at 370 nm exhibits a sharp emission band at 453 nm and a weak shoulder at 564 nm. The positions of emission bands remain unchanged when λ_{ex} is varied between (λ_{ex}- 10) and (λ_{ex}+ 10) nm (Fig. 3.15). The calculated values of the fluorescence quantum yields (Φ_s) are 0.41 and 0.40 for **1** and **2**, respectively.

Table 3.3 Electronic absorption and emission spectra of **1**-**2**.

	UV-vis[a]λ_{max}; [b]ε ($M^{-1}cm^{-1}$)		Emission (nm)	Δν[c], (nm)	Φ_s	[d]E_{Ox} (V), [e]i_{ac} (μA)	[f]FT-IR, [g](cm^{-1})
1	231(8.82×10^4), (4.62×10^4), (1.3×10^4)	276 **370**	430	60	0.41	0.514, -7.109	3430(br) [ν(O-H)], 2984 [ν(C-H)], 1642(vs) [ν (H-O-H)bending], 1550 [ν(C=N)]
2	231(6.14×10^4), (2.94×10^4), (8.0×10^3)	276 **370**	453	83	0.40	0.485, -2.334	3435(br) [ν(O-H)], 2984 [ν(C-H)], 1644 [ν_{as}(OCO)], 1551 [ν(C=N)], 1414 [ν_s(OCO)]

Bold number indicates the excitation wavelengths. [a] Wavelength in nanometer, [b] Molar extinction coefficient in $M^{-1}cm^{-1}$ in methanol solvent. [c] Stoke shift, [d] Methanol solution (supporting electrolyte NEt_4ClO_4, working electrode glassy carbon, reference electrode Ag/AgCl, scan rate 100 mV/s), [e] Anodic current, [f] in KBr pellet, [g] wave number in cm^{-1}.

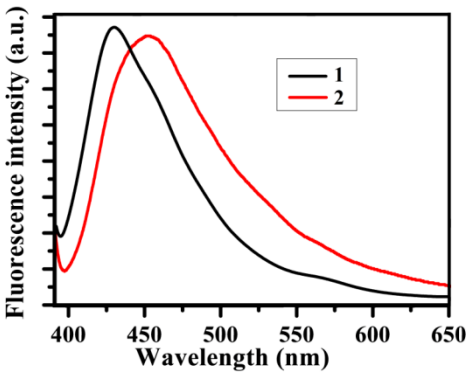

Fig. 3.15 Fluorescence spectra of complexes**1-2** (λ_{ex},370 nm, excitation and emission slit width = 5 nm).

3.3.5 ESI mass spectroscopy

ESI-mass spectra (Figs. 3.16, 3.17) of complexes show peaks at m/z = 1231.98 and 1231.31 for complexes **1** and **2**, respectively. The mass spectral peaks corresponds to the cationic unit $[Cu_4(L)_4(H_2O)_2]^{\cdot+}$ (calc. m/z = 1231.33 for both **1** and **2**). This result indicates that tetranuclear copper clusters are stable in solution.

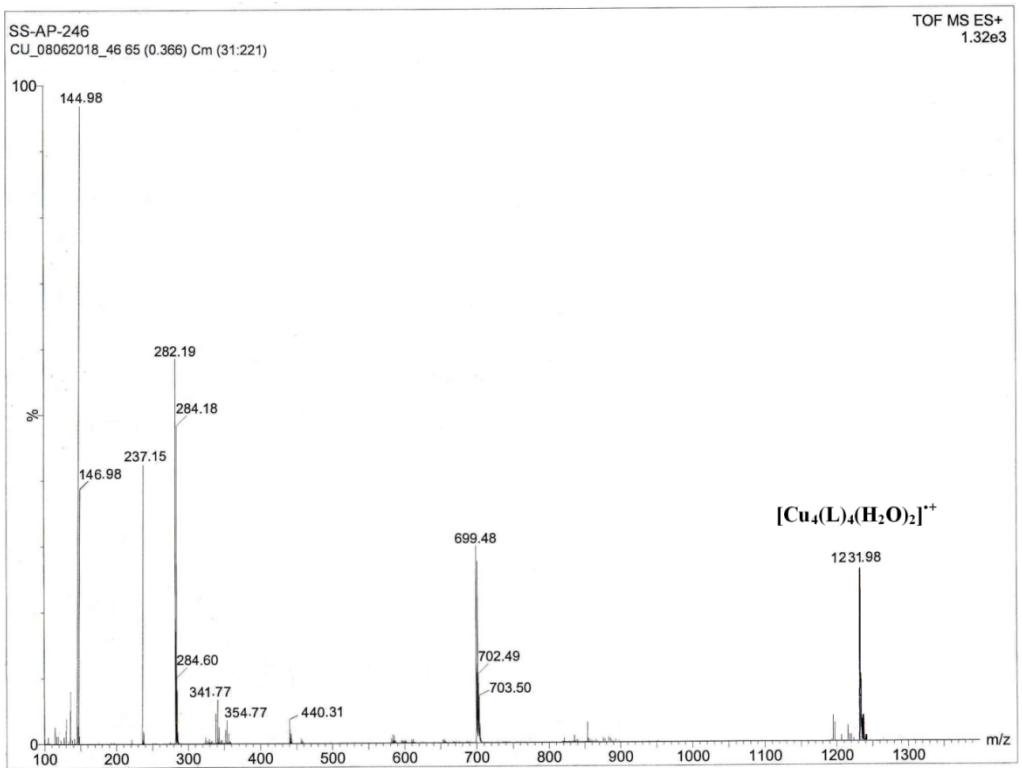

Fig. 3.16 ESI-mass spectrum of **1.**

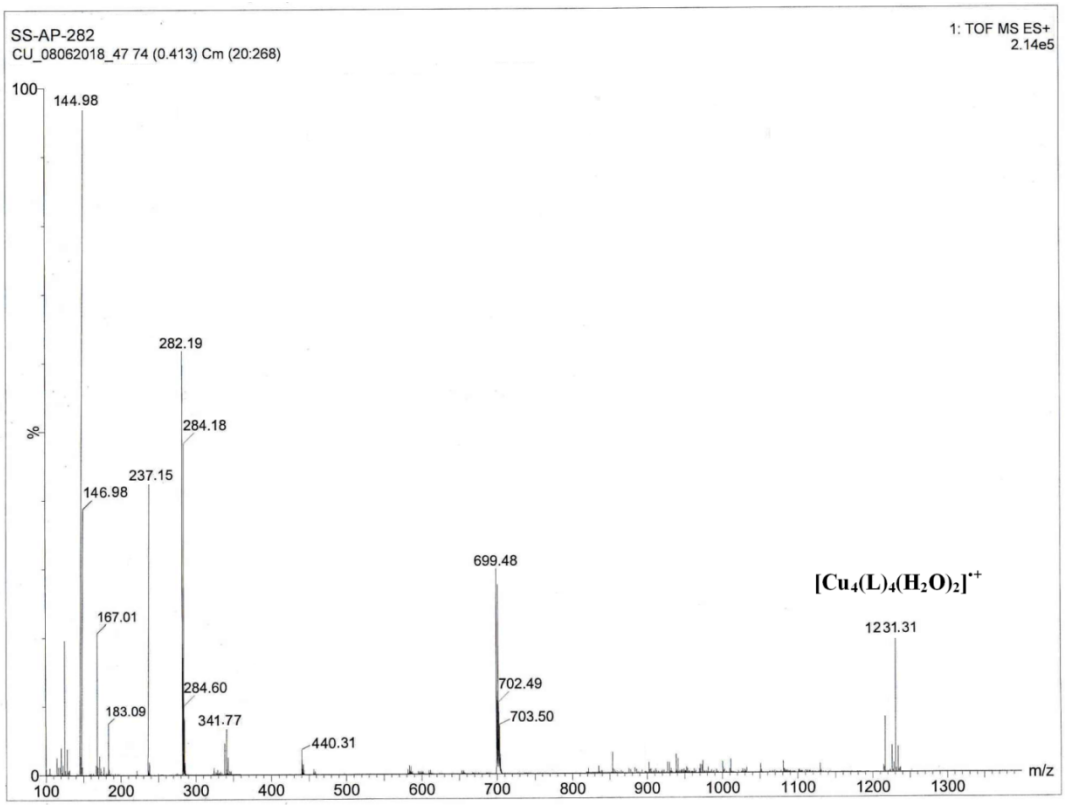

Fig. 3.17 ESI-mass spectrum of **2.**

3.3.6 Protein binding studies

A Study of the interaction of the complexes with serum albumins has been performed using Uv-vis absorption and fluorescence spectroscopic techniques.

Absorption spectral studies

The changes in the electronic absorption spectra of BSA (3 ml, 0.475 µM aqueous solution) and HSA (3 ml, 0.316 µM aqueous solution) after gradual addition (20 µL, 0.3475 mmol) of the complex solutions (at pH 7.2 using HEPPES buffer) at a temperature of 300 K are shown in Figs. 3.18 and 3.19. The absorption intensities for both BSA and HSA were enhanced with a little blue shift (2 nm for **1**; 3 nm for **2**). The shift of the electronic spectral band revealed the existence of a static interaction between the SAs and the complexes [3.36]. The apparent association constants

(K_a) were calculated from the 1/[complex] vs 1/(A_{abs}-A_0) plot (Fig. 3.20) using the following equation.

$$\frac{1}{(A_{obs} - A_0)} = \frac{1}{(A_c - A_0)} + \frac{1}{K_a(A_c - A_0)[complex]}$$

The values of the apparent association constant (K_a) are depicted in Table 3.4. The order of the association constant values are comparable to those reported for copper(II)-Schiff base complexes [3.37].

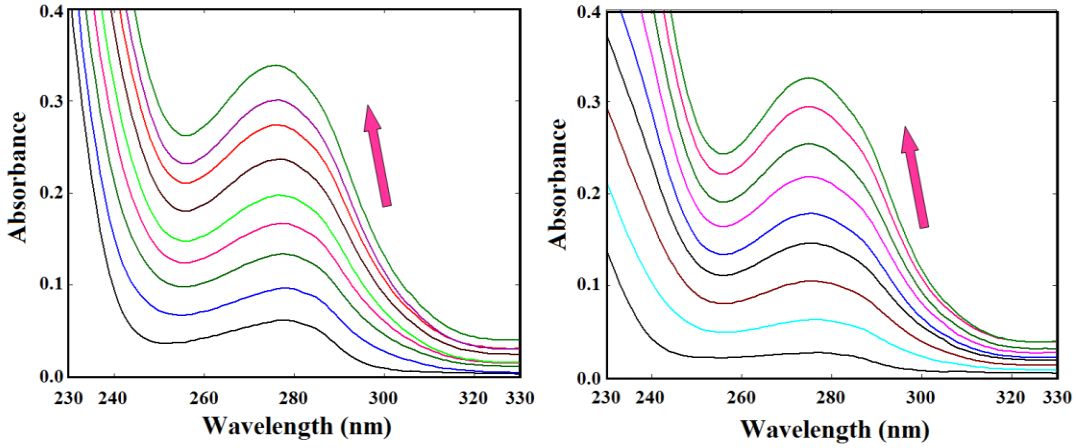

Fig. 3.18 UV-Vis absorption spectra BSA (left) and HSA (right) in the presence of increasing amounts (20 µL 0.755 µM) of complex **1**.

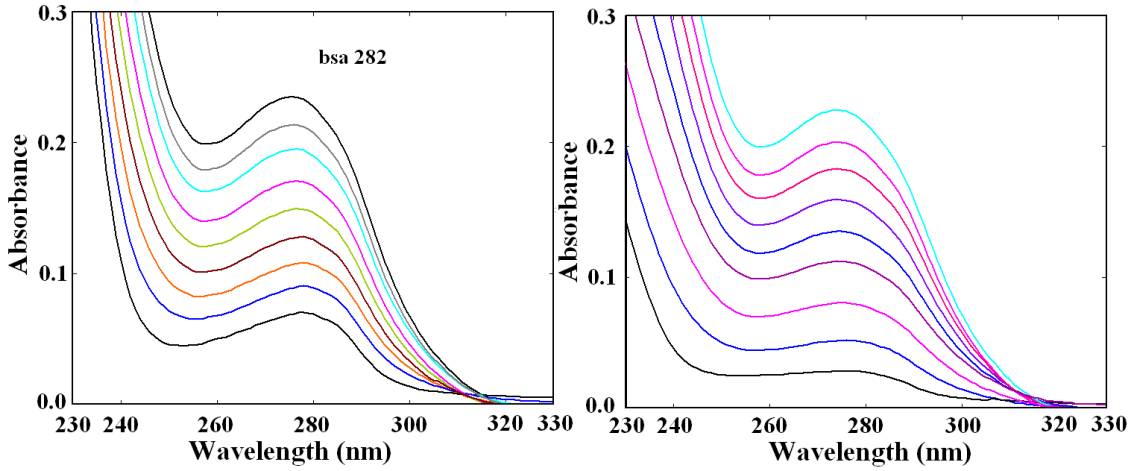

Fig. 3.19 UV-Vis absorption spectra BSA (left) and HSA (right) in the presence of increasing amounts (20 µL 0.755 µM) of complex **2**.

Table 3.4 Quenching constant (K_q), binding constant (K_{bin}), number of binding sites (n) and the values of apparent association constant (K_a) for the interactions of complexes **1-2** with BSA/HSA.

	Complexes	$K_{sv}(M^{-1})$	K_q ($M^{-1}S^{-1}$)	K_{bin} (M^{-1})	n	K_a (M^{-1})
BSA	**1**	$9.51(\pm0.09)\times10^4$	$1.90(\pm0.09)\times10^{13}$	$8.51(\pm0.01)\times10^4$	0.79	$9.50(\pm0.07)\times10^2$
	2	$7.99(\pm0.01)\times10^4$	$1.59(\pm0.01)\times10^{13}$	$7.58(\pm0.02)\times10^4$	0.73	$6.63(\pm0.07)\times10^2$
HSA	**1**	$7.45(\pm0.07)\times10^4$	$1.49(\pm0.07)\times10^{13}$	$7.17(\pm0.02)\times10^4$	0.83	$6.19(\pm0.09)\times10^3$
	2	$5.12(\pm0.06)\times10^4$	$1.02(\pm0.06)\times10^{13}$	$6.30(\pm0.03)\times10^4$	0.76	$3.47(\pm0.11)\times10^3$

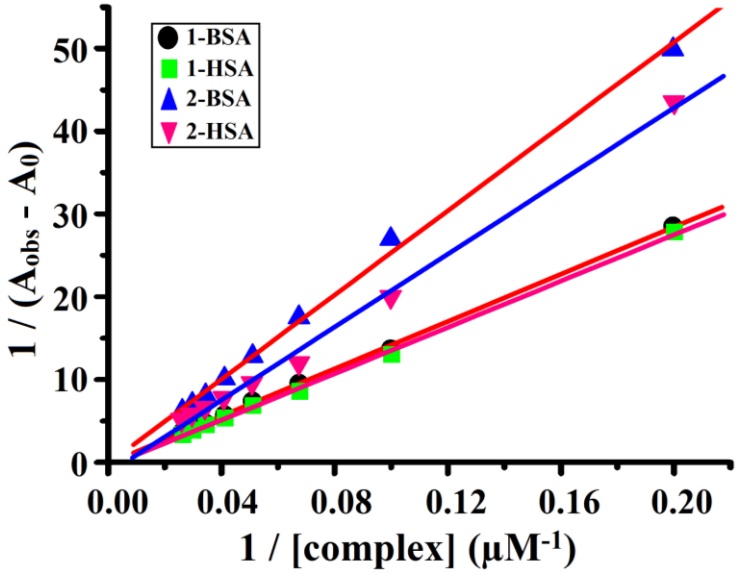

Fig. 3.20 Plot of 1/[complex] vs 1/ (A_{obs}-A_0) for interaction of complexes **1-2** with serum albumins.

Fluorescence spectroscopic studies

The changes in the emission spectra of the serum albumins upon addition of increasing concentrations (0-11.2 μM) of complexes are shown in Fig. 3.21. The fluorescence intensity of BSA at ~340 nm was quenched with a small blue shift (52.80%, 4 nm for **1**; 46.81%, 3 nm for **2**). The 330 nm emission band of HSA was also quenched with a blue shift (45.47%, 4 nm for **1**; 36.90%, 4 nm for **2**). The blue shift primarily arises due to the presence of the active site of the protein in a hydrophobic environment [3.38]. From this observation it is clear that some interaction is taking place between the complexes and SAs. From the Stern-Volmer equation

[3.22] a linear relationship was obtained for the titration of serum albumins using the complexes as a quencher (inset of Fig. 3.21). The calculated values of the Stern-Volmer quenching constant (K_{SV}) and the quenching rate constant (K_q) (Table 3.4) for BSA binding are K_{SV} = 9.51 (±0.09) $\times 10^4$ M^{-1}, K_q = 1.90 (±0.09) $\times 10^{13}$ $M^{-1}S^{-1}$ for **1** and K_{SV} = 7.99 (±0.01)$\times 10^4$ M^{-1}, K_q = 1.59(±0.01) $\times 10^{13}$ $M^{-1}S^{-1}$ for **2**. Whereas for HSA binding K_{SV} = 7.45(±0.07)$\times 10^4$ M^{-1}, K_q = 1.49(±0.07) $\times 10^{13}$ $M^{-1}S^{-1}$ for **1** and K_{SV} = 5.12(±0.06)$\times 10^4$ M^{-1}, K_q = 1.02(±0.06) $\times 10^{13}$ $M^{-1}S^{-1}$ for **2**. The magnitudes of K_{SV} values indicate that both the complexes have a good fluorescence quenching ability.

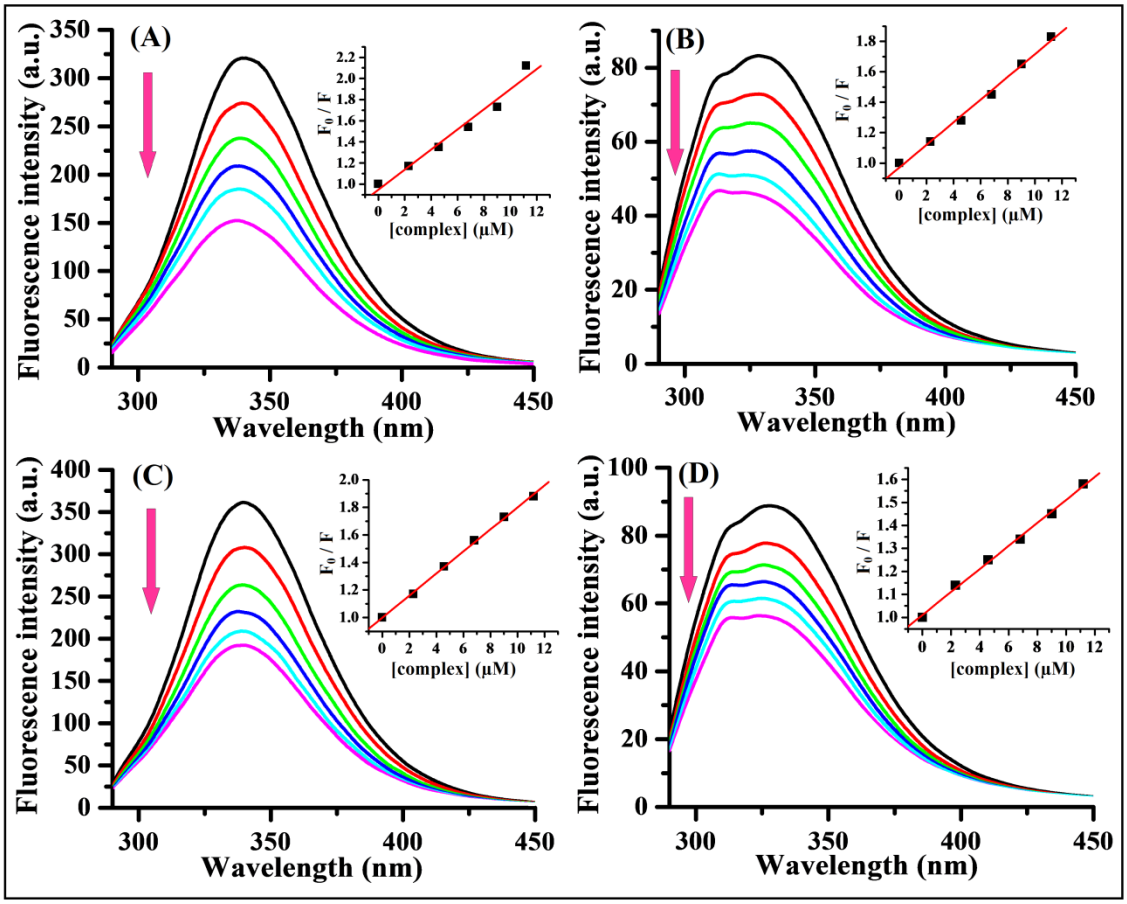

Fig. 3.21 Fluorescence spectra of BSA (λ_{ex} = 280 nm; λ_{em} = 340 nm) and HSA (λ_{ex} = 280 nm; λ_{em} = 330 nm) in the presence of increasing amounts of complex **1** [(A) for BSA, (B) for HSA] and complex **2** [(C) for BSA, (D) for HSA]. Arrows show the emission intensity changes upon increasing complex concentration. Inset: Stern-Volmer plot.

The Uv-vis absorption spectra of the SAs show a noticeable change in the presence of the complexes. This indicates the presence of a static interaction between the SAs and complexes **1** and **2**. To have a deep insight into the quenching sequence, the equilibrium binding constant (K_{bin}) and number of binding site (n) were also evaluated from the plot of log [(F_o- F)/F] versus log [complex] (Fig. 3.22) using the Scatchard equation [3.29], binding constant (K_{bin}) and the number of binding sites per albumin (n) for the complexes are given in Table 3.4. The calculated value of n is around 1 for all the complexes, indicating the existence of just a single binding site in SAs for the complexes.

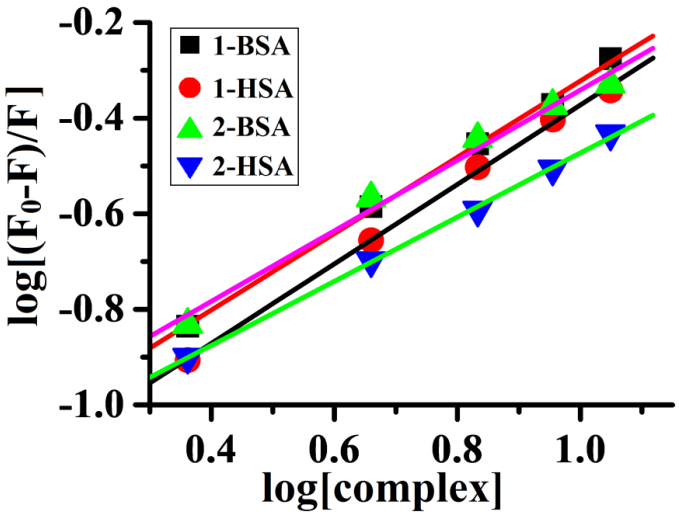

Fig. 3.22 Scatchard plots for complexes **1-2** with BSA / HSA. ([complex] is the total concentration of added complex).

3.3.7 Interaction with Calf-Thymus DNA

Metal complexes bind to double-stranded DNA via covalent or non-covalent interactions. Non-covalent interactions with DNA involve three binding modes: intercalative binding, groove binding and electrostatic interactions [3.39]. Here the interactions of the complexes with CT-DNA were studied with Uv-vis absorption and ethidium bromide (EB) displacement studies.

Uv-vis absorption spectral studies

The absorption spectra of the complexes in the absence and presence of CT-DNA are shown in Fig. 3.23. Addition of increasing amounts (0 - 15.48 μM) of CT-DNA results increase in the absorption intensity of complexes and in a significant shift in the band position. For **1**, the absorption bands at 231, 276 and 370 nm showed hyperchromism with 4 nm red, 8 nm blue and 5 nm red shifts, respectively. For **2**, the bands at 231, 276 and 370 nm showed hyperchromism with 6 nm red, 13 nm blue and 4 nm red shifts, respectively. From the plots of [DNA] / (ε_a-ε_f) versus [DNA] (inset of Fig. 3.23), linear relationship were obtained, and the intrinsic binding constants (K_{ib}) were calculated from the ratio of the slope and the intercept. The calculated values of K_{ib} are 1.25(±0.22) × 10^4 and 8.77(±0.10) × 10^3 M^{-1} (Table 3.5) for **1**and **2** respectively. These results indicate that both the new copper complexes bind to the CT-DNA helix.

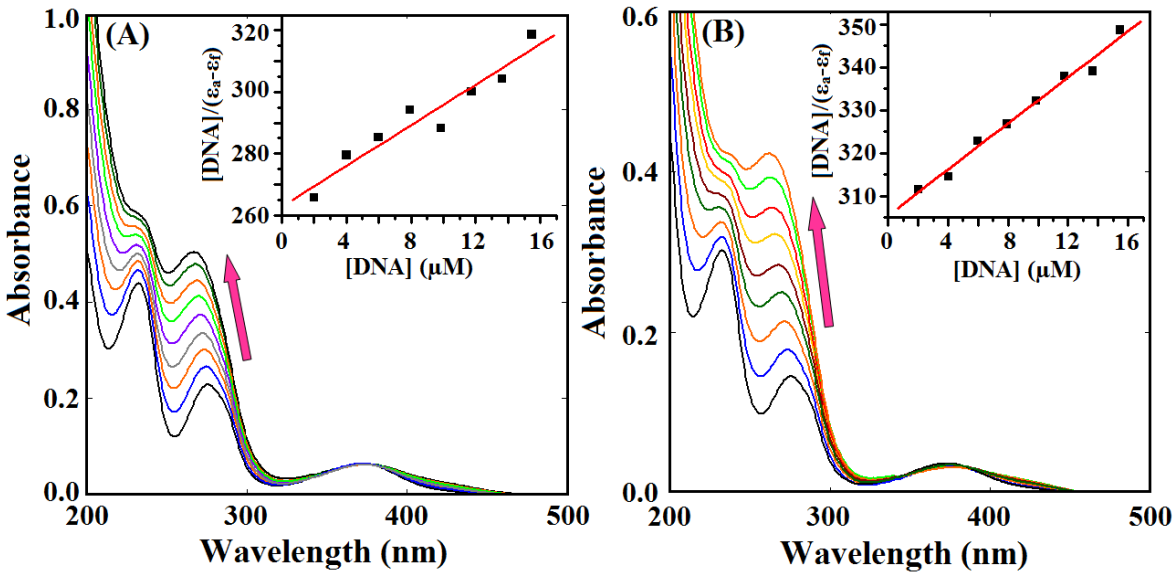

Fig. 3.23 Absorption spectra of complexes [(A) for **1;** and (B) for **2]** in the absence (black line) and in presence (other lines) of increasing amounts of CT-DNA, at room temperature. Inset: show the plots of [DNA]/(ε_a-ε_f) *vs.* [DNA]. The arrows show the absorbance change with increasing CT-DNA concentration.

Competitive binding between ethidium bromide and the complexes

Absorption titration studies indicated that **1** and **2** effectively bind with CT-DNA. The nature of binding between complexes and CT-DNA were also studied adopting ethidium bromide (EB) displacement experiments. EB is a planer, cationic dye, and it is one of the most sensitive fluorescence probes which can bind to DNA through intercalation [3.40]. The changes of the emission spectra of EB bounded CT-DNA with increasing concentration of the complexes are shown in Fig. 3.24. Due to the displacement of EB from the CT-DNA sequence by complexes, the fluorescence intensity decreases as the number of binding sites on the DNA available for EB are also reduced. It is of note that **1** and **2** do not show any significant fluorescence when excited at 500 nm in the presence of CT-DNA. Furthermore the addition of the complexes to a solution containing only EB do not show any quenching of the free EB fluorescence.

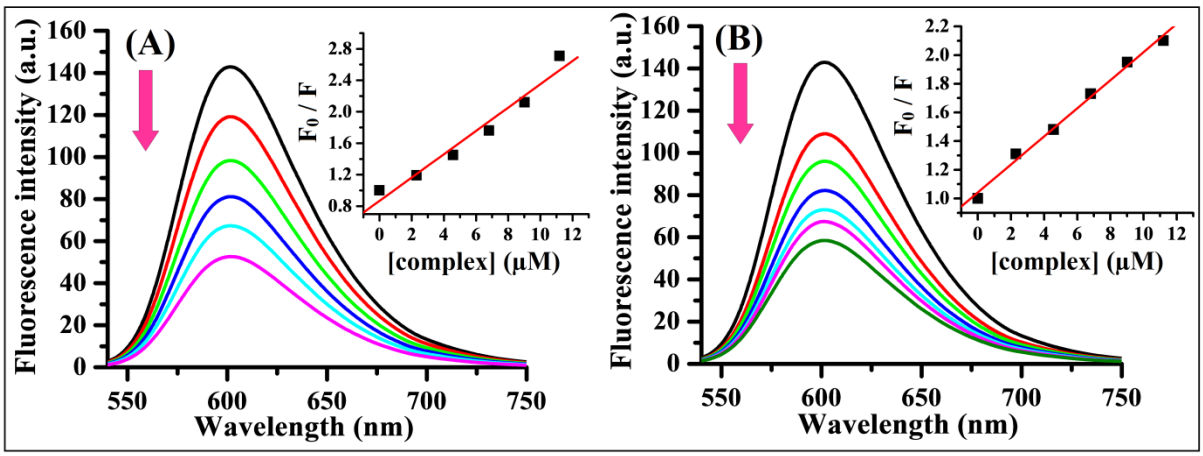

Fig. 3.24 Effect of addition of complexes **1** (A) and **2** (B) on the emission intensity of EB bounded CT-DNA. Inset: Stern-Volmer plots of fluorescence titrations.

On gradual addition of the complexes (20μL, 0.3475 μM) to an EB bounded CT-DNA solution, the quenching of the emission of EB bounded CT-DNA was observed. The 602 nm emission band exhibited hypochromism up to 63.13% (for **1**) and 52.53% (for **2**) of the initial fluorescence

intensity. The observed decrease in fluorescence intensity is due to displacement of EB from CT-DNA binding sites by the complexes [3.41].

Table 3.5 Electronic spectral parameters of the complexes **1-2** bound to CT-DNA.

	λ_{max} (nm)	change in emission	Δε (%)	$K_{sv}(M^{-1})$	$K_{ib}(M^{-1})$	K_{app} (M^{-1})
1	602	hypochromism	63.13	$1.483(\pm0.11)\times10^5$	$1.25(\pm0.22)\times10^4$	8.86×10^5
2	602	hypochromism	59.09	$9.78(\pm0.08)\times10^4$	$8.77(\pm0.10)\times10^3$	7.14×10^5

The Stern-Volmer plots (inset of Fig. 3.24) for these fluorescence titration show straight line (R = 0.9796, 0.9963). The K_{sv} values have been derived from the slope of F_0/F vs [complex] plots, and the values are 1.483 (±0.11) × 10^5 (for **1**) and 9.78 (±0.08) × 10^4 M^{-1} (for **2**). The apparent DNA binding constant (K_{app}) values were calculated using the equation [3.36a]

$$K_{EB}[EB] = K_{app}[complex]$$

where the complex concentration is the value at a 50% reduction in the fluorescence intensity of EB, K_{EB} (1.0×10^7 M^{-1}) is the DNA binding constant of EB, [EB] is the concentration of EB (8 μM). The K_{app} values were found to be 8.86×10^5 and 7.14×10^5 for **1** and **2**, respectively and these results are given in Table 3.5. From these observed data, it is seen that both the complexes have comparable binding affinities. A comparison (Table 3.6) of the kinetic parameters of the CT-DNA interaction of the present compounds with reported tetranuclear cubane core (Cu_4O_4) complexes, $[Cu_4(L^1)_4]$ [3g] (H_2L^1; Schiff base of 1-amino-2-propanol and salicylaldehyde) and $\{[Cu_4(\mu\text{-}L^2)_2(\mu_{1,1,3,3}\text{-}O_2CH)](OH)\cdot6H_2O\}$[3h] ($H_3L^2$;1,3-bis[3-aza-3-(1-methyl-3-oxobut-1-enyl)prop-3-en-1-yl]-2-(2-hydroxyphenyl)-1, 3-imidazolidine) show that **1** and **2** have comparable binding affinities with reported compounds.

Table 3.6 Kinetic parameters of the interaction of Cu(II) cubane compounds with CT-DNA.

Compound	K_{ib}	Ksv	Ref.
$[Cu_4(L)_2(HL)_2(H_2O)_2]\cdot 2(ClO_4)\cdot DMF$ (**1**)	1.25×10^4	1.483×10^5	This work
$[Cu_4(L)_2(HL)_2(H_2O)_2]\cdot(tp)$ (**2**)	8.77×10^3	9.78×10^4	This work
$Cu_4(L^1)_4$	4.50×10^3	-	[3.3g]
$[Cu_4(\mu\text{-}L^2)_2(\mu_{1,1,3,3}\text{-}O_2CH)](OH)\cdot 6H_2O$	3.37×10^4	4.73×10^4	[3.3h]
$[Cu_4((HL^3)_2(H_2L^3)_2(H_2O)(C_2H_5OH)]\cdot 2(ClO_4)\cdot 2(C_2H_5OH)$	1.35×10^4	1.69	[3.3i]
$[Cu_4(H_2L^4)_4\cdot 2H_2O]\cdot 5H_2O$	1.48×10^4	-	[3.3j]
$[Cu_4(H_2L^4)_4\cdot 4H_2O]$	2.54×10^4	-	[3.3j]

H_2L^1 = Schiff base of 1-amino-2-propanol and salicylaldehyde; H_3L^2 =1,3-bis [3-aza-3-(1- methyl-3-oxobut-1-enyl)prop-3-en-1-yl]-2-(2-hydroxyphenyl)- 1,3-imidazolidine; H_3L^3 = 2-ethyl-2-((2-hydroxy-3-methoxybenzylideneamino)propane-1,3-diol); H_4L^4 = 2-[(2-Hydroxy-3-methoxy-benzylidene)-amino]-2-hydroxymethyl-propane-1,3-diol.

3.3.8 Redox properties of complexes

The electrochemical behavior of the complexes was investigated in methanol solution by cyclic voltammetry in the potential range between 0.3 and 0.7 V. The voltammetric data are collected in Table 3.3 and the voltammograms are displayed in Fig. 3.25. The cyclic voltammograms show the irreversible oxidation processes at 0.51 and 0.48 V for **1** and **2**, respectively.

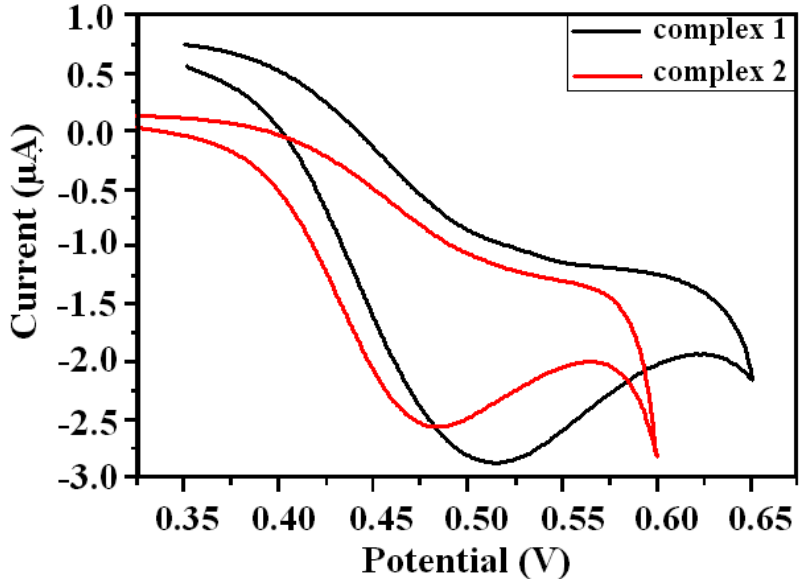

Fig. 3.25 Cyclic voltammograms of **1** (black) and **2** (red).

3.4 **Conclusion**

In summary, we have presented here the synthesis, crystal structure, DNA and protein binding studies of two 2-ethoxy-6-[(1-hydroxymethyl-propylimino)-methyl]-phenol (H_2L) ligand based copper(II) complexes (**1** and **2**). The X-ray structural analysis shows that in both complexes the H_2L ligand is present in its mono (HL^-) and dianionic (L^{2-}) forms with the μ_2-η^1:η^1:η^1:η^2-*O,O,N,O and* μ_3-η^1:η^1:η^3-*O,N,O* coordination modes, respectively. Both the complexes possess a double open [Cu_4O_4] cubane core structure and the only difference is the presence of lattice solvents and anions. Supramolecular C-H…π interactions results in the 2D and 3D supramolecular architectures of **1** and **2**, respectively. The CT-DNA and protein binding of the compounds were investigated using electronic absorption and emission spectroscopic techniques. The compounds bind effectively with CT-DNA in the order 10^4 M^{-1} through a non-intercalative interaction. A fluorescence spectroscopic study evidences that the interactions of **1** and **2** with serum albumins occur through ground state association process.